Full-Wave Analysis of Nanoscale Optical Trapping

Edward P. Furlani* and Alexander Baev
The Institute for Lasers, Photonics and Biophotonics, University at Buffalo
*Corresponding author: 432 Natural Sciences Complex, Buffalo, NY 14260-3000, efurlani@buffalo.edu

Abstract: We present a study of plasmonic-based optical trapping of neutral sub-wavelength particles in proximity to illuminated metallic nanostructures. We compute the dipolar force on the particles using 3D full-wave electromagnetic analysis, and perform parametric studies of the force as a function of the incident wavelength and background medium.

Keywords: plasmonic nano-tweezers, optical nanotrapping, optical nanoparticle manipulation, plasmon-based optical manipulation

1. Introduction

The interest in optical manipulation is growing rapidly, especially for bio-applications where the manipulated objects include viruses, cells and intracellular organelles [1-5]. While micron and sub-micron particles can be manipulated using conventional laser tweezers, the resolution of this approach is diffraction-limited (~250 nm), and the high optical power and focusing of the laser beam can limit the exposure time of a trapped specimen. These limitations can be overcome using plasmonics [6,7], wherein sub-wavelength particles are manipulated using the enhanced near-field gradients that exist around illuminated metallic nanostructures. In this presentation we discuss plasmon-based optical trapping of dielectric nanoparticles in proximity to illuminated metallic nanopillars (Fig. 1).

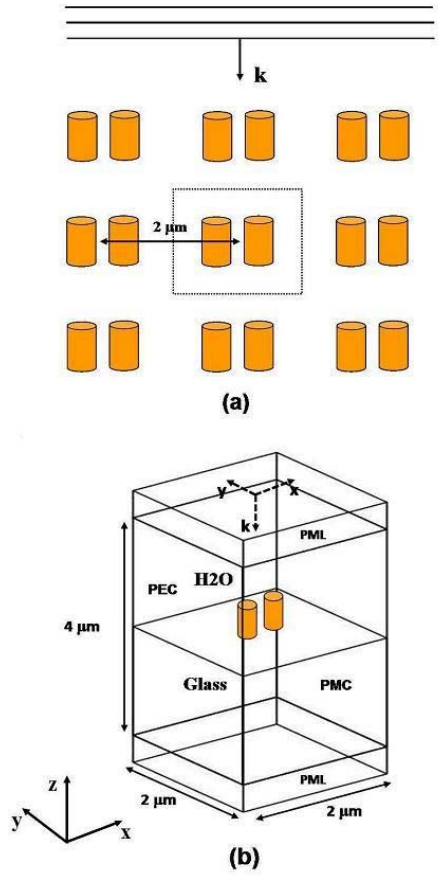

Figure 1. Plasmonic nanotrapping system: (a) illuminated array of metallic nanopillar pairs, (b) computational domain with boundary conditions.

2. The Numerical Model

We use the COMSOL RF solver to compute the field distribution and dipolar force for the nanostructured system shown in Fig. 1a. This illustrates an array of paired gold nanopillars illuminated from above. In our actual model the nanopillars are on a glass substrate which is covered by H2O. The computational domain for the analysis is shown in Fig. 1b. It spans 5 μm in the direction of propagation (z-axis), and 2 μm in both the x and y directions (Fig. 1b). The nanopillars are identical, and the pair is centered on the x-y plane (z=0) and aligned along the x-axis. The nanopillars have a diameter and height of 200 nm. We apply perfectly matched layers (PMLs) at the top and bottom of the computational domain to reduce backscatter at these boundaries. The PMLs are 0.5 μm thick, which leaves 4 μm of physical domain along the z-axis. We impose perfect electric conductor (PEC) conditions at the boundaries perpendicular to the E field at $x = \pm 1$ μm, and perfect magnetic conductor (PMC) conditions at the boundaries perpendicular to the H field at $y = \pm 1$ μm. These boundary conditions ensure normal incidence of the respective fields at the boundaries transverse

to the direction of propagation. They account for a 2D array of nanopillars pairs with a center-to-center lattice spacing of 2 μm in both the x and y directions. Thus, we are studying the field due to a single element of a 2D array of nanopillar pairs.

We analyze the optical trapping of sub-wavelength particles by computing the time-averaged dipolar force,

$$\langle F_i \rangle = \frac{1}{2} \sum_j \mathrm{Re}\left[\alpha E_{0j} \partial^i \left(E_{0j} \right)^* \right], \quad (1)$$

where E_{0j} $(j = 1,2,3)$ are the Cartesian components of the computed optical field, and

$$\alpha = \frac{4\pi \alpha_0 \varepsilon_0}{\left[1 - \alpha_0 \left(\frac{k^2}{a} - \frac{2}{3} ik^3 \right) \right]} \quad (2)$$

is the polarizability of the particle, where $\alpha_0 = R_p^3 \frac{\varepsilon_p - \varepsilon_m}{\varepsilon_p + 2\varepsilon_m}$ [8]. Here, R_p and ε_p are the radius and relative permittivity of the particle, respectively, and ε_m is relative permittivity of the ambient medium (1 for air). The imaginary term in α accounts for the scattering force on a particle, and it is important to note that the sign of this term (i.e. $\pm \frac{2}{3} ik^3$) depends on the convention used in the time-harmonic analysis, i.e. $\exp(i\omega t)$ or $\exp(-i\omega t)$ [10]. The RF solver uses the $\exp(i\omega t)$ convention, which is compatible with Eq. (2).

The dielectric permittivity of the gold nanopillars is modeled using an analytical expression [11,12]

$$\varepsilon_{\mathrm{Au}}(\omega) = \varepsilon_\infty - \frac{\omega_p^2}{\left(\omega^2 + i\Gamma\omega \right)} + G_1(\omega) + G_2(\omega), \quad (3)$$

where the first and second terms are contributions from a Drude model, and $G_1(\omega)$ and $G_2(\omega)$ are contributions from interband transitions, which are of the form

$$G_k(\omega) = C_k \left[\frac{e^{i\phi_k}}{\left(\omega_k - \omega - i\Gamma_k \right)} + \frac{e^{-i\phi_k}}{\left(\omega_k + \omega + i\Gamma_k \right)} \right] \quad (4)$$

We compute the dipolar force exerted on a dielectric spherical particle above the pillars as a function of the wavelength of the illuminating wave. We illuminate the nanopillars with a downward directed uniform TEM plane wave with the E field along the x-axis. The incident field is generated by a time-harmonic surface current source positioned in the x-y plane 2 μm above the top surface of the semi-shell, i.e. at z = 2 um (immediately below the upper PML). The magnitude of the surface current is chosen to provide a plane wave with a field magnitude of $E_x = 2 \times 10^6$ V/m. The FEA model comprised 57,666 cubic vector elements with 1,094,940 degrees of freedom.

3. Results and Discussion

We perform an initial simulation using an incident wavelength of λ = 700 nm. A plot of the negative time-averaged electric energy density $-\langle W_e \rangle$ at 620 nm above the surface of the substrate is shown in Fig. 2. This function is proportional to the dipolar gradient force potential $-|E|^2$, and we use it to identify potential regions of particle trapping.

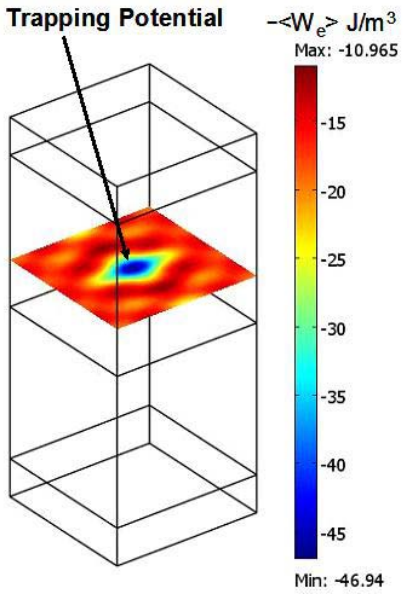

Figure 2. TEM full-wave analysis at λ = 700 nm: time-averaged electric energy density -<W_e> in x-y plane 620 nm above the semi-shell.

Specifically, the plot in Fig. 2 exhibits a central minimum, which implies particle trapping/confinement in this plane, i.e. the lateral optical forces act to keep a dielectric particle

near the z-axis. We explore this in more detail below.

Next, we compute the time-averaged axial dipolar force F_z on nanoparticles along the z-axis as shown in Fig. 3. We assume that all particles have a relative dielectric permittivity $\varepsilon_p = 2.25$ and a radius $R_p = 100$ nm. We compute the force for three different wavelengths $\lambda = 600$, 700 and 800 nm (Fig. 4). Axial trapping points occur where F_z changes sign, i.e. from positive below the point to negative above it. Thus, below the point F_z acts to move the particle upward, whereas above the point F_z acts to move the particle downward. In Fig. 4 we identify such a points near z = 620 nm for $\lambda = 700$ nm.

It is instructive to study the trapping force induced by the nanopillars when they are immersed in different media. Specifically, we

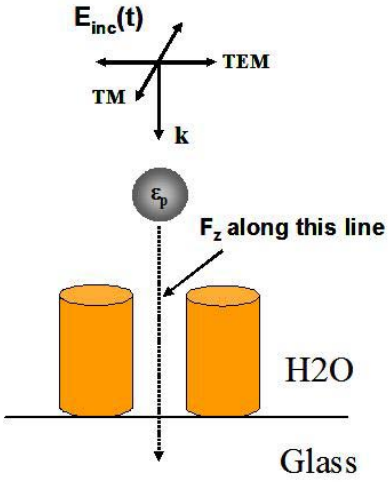

Figure 3. Time-averaged dipolar force computed along the z-axis above the substrate.

consider the force on the particle described above when the pillars are isolated in air and water, respectively (Fig. 5). The changes of the ambient medium modify the axial dependence of the dipolar force. When the pillars are isolated in air, the force exhibits a resonance at a wavelength $\lambda = 600$ nm and the trapping position is 0.4 μm (Fig. 5a). When the ambient medium is water the resonance of the force shifts to $\lambda = 800$ nm (Fig. 5b), although the trapping position at 0.2 μm is not accessible to the particle, i.e. it cannot squeeze between the pillars. The trapping position for the wavelength of 600 nm previously observed at 0.4 μm shifts to 0.3 μm. Note that the magnitude of the dipolar force

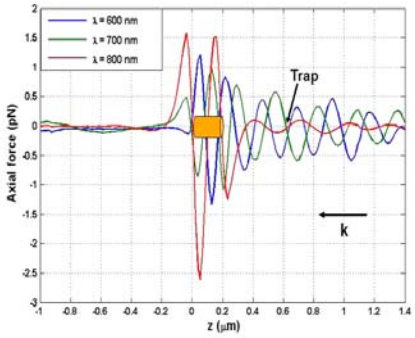

Figure 4. Time-averaged dipolar force computed along the z-axis above the substrate for $\lambda = 600$, 700 and 800 nm.

decreases because the dielectric contrast between the particle and the ambient medium decreases. When the pillars are placed on a glass substrate, the magnitude of the force at 800 nm increases (Fig. 3) compared to the case without the substrate (Fig. 5). In addition, a trapping site at approximately 0.5 μm can be observed. It is therefore clear that the axial trapping position of a particle can be controlled by tuning the wavelength of the incoming light.

To ensure that a particle is trapped at a point, the optical restoring force needs to be greater than the gravitational and Langevin forces. According to our estimations, the Langevin force

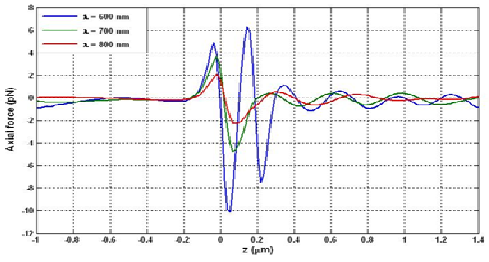

(a)

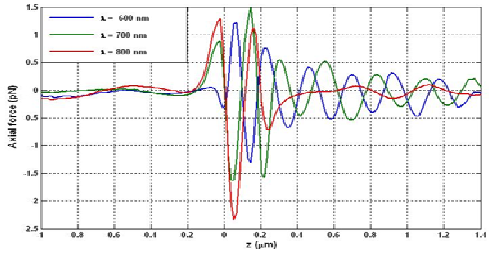

(b)

Figure 5. Dipolar force exerted on a 100 nm radius dielectric particle: (a) nanopilllars in air; (b) nanopillars in water.

is much smaller than the optical trapping force when the particles are in water. Thus, aqueous environments, typically used for experiments with biological agents, are suitable for nanoscale optical trapping experiments.

4. Conclusions

Plasmonic-based optical trapping is its infancy and growing rapidly. Research in this area will significantly advance fundamental understanding in fields such as nanophotonics and biophotonics. Plasmonic optical trapping has advantages over conventional laser trapping in that it enables a higher spatial resolution, lower trapping energy, parallel trapping of multiple specimens, and a higher level of system integration, which holds potential for Lab-on-Chip applications. Novel plasmonic trapping structures and systems can be designed and optimized using the COMSOL RF solver. This capability will facilitate the development of a new generation of systems for manipulating matter at the nanoscale.

References

[1] A. Ashkin, Optical trapping and manipulation of neutral particles using lasers, *Proc. Natl. Acad. Sci.* **94**, 4853 (1997).

[2] C.L. Kuyper and D.T. Chiu, Optical trapping: A versatile technique for biomanipulation, *Appl. Spectrosc*. **56,** 295A, (2002).

[3] A. Ashkin and J.M. Dziedzic, Optical trapping and manipulation of viruses and bacteria, *Science* **235**, 1517 (1987).

[4] K Svoboda and S.M. Block, Biological applications of optical forces, *Annu. Rev. Biophys. Biomol. Struct.* **23,** 247 (1994).

[5] P.N. Prasad, Introduction to biophotonics, John Wiley & Sons, NJ (2003).

[6] H.A. Atwater, The Promise of plasmonics, *Scientific American* **296,** 56 (2007).

[7] P.N. Prasad, Nanophotonics, John Wiley & Sons, NJ (2004).

[8] P.C. Chaumet and M. Nieto-Vesperinas, Time-averaged total force on a dipolar sphere in an electromagnetic field**,** *Opt. Lett.* **25**, 1065 (2000).

[10] Private communication with P.C. Chaumet.

[11] P.G. Etchegoin, E.C. Le Ru, and M. Meyer, An analytic model for the optical properties of gold, *J. Chem. Phys.* **125**, 164705 (2006).

[12] P.G. Etchegoin, E.C. Le Ru and M. Meyer, Erratum: An analytic model for the optical properties of gold, *J. Chem. Phys.* 125, 164705 (2006), *J. Chem. Phys.* **127**, 189901 (2007).